Journal of Power Sources 220 (2012) 47–53

Contents lists available at SciVerse ScienceDirect

Journal of Power Sources

journal homepage: www.elsevier.com/locate/jpowsour

Synthesis and electrochemical performance of LiV_3O_8/polyaniline as cathode material for the lithium battery

Xuan-Wen Gao [a], Jia-Zhao Wang [a,*], Shu-Lei Chou [a], Hua-Kun Liu [a,b]

[a] Institute for Superconducting and Electronic Materials, University of Wollongong, Wollongong, NSW 2522, Australia
[b] ARC Center of Excellence for Electromaterials Science University of Wollongong, University of Wollongong, Wollongong, NSW 2522, Australia

HIGHLIGHTS

- LiV_3O_8–polyaniline nanocomposites synthesized via chemical oxidative polymerization.
- Polyaniline coating can prevent the dissolution into the $LiPF_6$ electrode that occurs in LiV_3O_8 during cycling.
- Polyaniline coating increases the electrical conductivity in LiV_3O_8 electrode.
- The composite has higher high-rate capacities and capacity retention than pure LiV_3O_8.

ARTICLE INFO

Article history:
Received 1 May 2012
Received in revised form
12 July 2012
Accepted 31 July 2012
Available online 8 August 2012

Keywords:
LiV_3O_8
Conducting polymer
Composite
Polyaniline
Cathode material

ABSTRACT

LiV_3O_8–polyaniline nanocomposites have been synthesized via chemical oxidative polymerization directed by the anionic surfactant sodium dodecyl benzene sulfate. The polyaniline particles are uniformly coated on the LiV_3O_8 nanorods. The composite with 12 wt.% polyaniline retains a discharge capacity of 204 mAh g^{-1} after 100 cycles and had better rate capability (175 mAh g^{-1} at 2 C and 145 mAh g^{-1} at 4 C) than the bare LiV_3O_8 electrode in the potential range of 1.5–4.0 V. The polyaniline coating can buffer the dissolution into the $LiPF_6$ electrode that occurs in LiV_3O_8 during cycling. The charge transfer resistance of the composite electrode was much lower than that of the bare LiV_3O_8 electrode, indicating that polyaniline coating significantly increases the electrical conductivity between the LiV_3O_8 nanorods. Polyaniline is a conductive binder which buffers the dissolution of LiV_3O_8 into the electrolyte and reduces the contact resistance among nanorods, so performance of the composite is significantly improved.

1. Introduction

The layered lithium vanadium oxide, LiV_3O_8 has received considerable attention as cathode material in rechargeable lithium batteries due to its excellent electrochemical performances: high specific energy density, high working voltage, high discharge capacity, good chemical stability in air, ease of fabrication and low cost [1–4]. It is well understood that the electrochemical properties of lithium vanadium oxide are largely depend on the preparation method. Therefore, many preparation methods have been studied to LiV_3O_8 with an aim to improve its electrochemical performance, such as spray pyrolysis method [5], sol–gel method [6–8], microwave-assisted synthesis [9], ultrasonic treatment [4] and hydrothermal synthesis [10]. Recently, Liu et al. [11] employed home-made VO_2 nanorods as the vanadium precursor to prepare the LiV_3O_8 cathode materials. The as-obtained single-crystalline LiV_3O_8 nanorods with high crystallinity greatly improved the stability of the crystallographic structure during cycling. It exhibited high initial discharge capacity of more than 300 mAh g^{-1} at current densities of 20 mA g^{-1}. Up to now, however, this kind of material was still suffering from the phase transformation and dissolution of small quantity of LiV_3O_8 in the electrolyte [12], which lead to low high-rate capacity and fast capacity fading with cycling.

Recently, coating with conducting polymers has been studied as an effective method to improve the electrical performance of cathode and anode materials in lithium-ion batteries. Conductive polymers are attractive additive materials for lithium-ion batteries, owing to their special electrochemical properties: (i) they can be charged and discharged by a redox reaction involving lithium ions or counter anions of the electrolyte; (ii) they have an influence on the overall phase-change rate; and (iii) they can connect isolated crystalline particles, preventing their agglomeration on the surface

* Corresponding author. Tel.: +61 2 4298 1478; fax: +61 2 4221 5731.
E-mail address: jiazhao@uow.edu.au (J.-Z. Wang).

0378-7753/$ – see front matter © 2012 Elsevier B.V. All rights reserved.
http://dx.doi.org/10.1016/j.jpowsour.2012.07.114

of electrodes. Moreover, conducting polymers can suppress the dissolution of active materials into the $LiPF_6$ electrolyte [13–15]. Up to now, many electrode materials combined with polymers, for example, SnO_2/polypyrrole [16], sulphur/polypyrrole [17], $LiMn_2O_4$/polypyrrole [14], $LiFePO_4$/polypyrrole [18,19], $LiFePO_4$/polyaniline [20], V_2O_5/polyaniline [21], and LiV_3O_8/polypyrrole [22,23] have been synthesized and have shown improved cycling performance in lithium cells. In our previous work, polypyrrole coated LiV_3O_8 exhibited improved cycling stability [22,23]. The rate capability, however, was not discussed in these studies. In this study, we have tried to investigate the effects of a conducting polymer on the high rate capability of LiV_3O_8 and to explore a possible new conducting polymer to improve the electrochemical performance of LiV_3O_8 cathode.

Among the various conductive polymers, polyaniline (PAn) has been used extensively because it can be easily produced with the desired morphology and structure by chemical reaction. It can promote electrolyte permeation into the surface of the active particles, and hence enhance Li^+ insertion/extraction during the charge/discharge process [20]. It is also superior to polypyrrole and polythiophene in energy density and durability [24]. In addition, polyaniline is electrochemically active in the range of 2.0–3.8 V [25], which overlaps the operative redox couple of LiV_3O_8. Therefore, polyaniline not only serves as a conductive binder-like carbon powder for LiV_3O_8 electrodes, but also participates as an active material. Herein, the LiV_3O_8 nanorods were coated with polyaniline via simple chemical oxidative polymerization directed by the anionic surfactant sodium dodecyl benzene sulfate (SDBS). The electrochemical properties of LiV_3O_8–PAn as cathode material were systematically investigated.

2. Experimental

2.1. Materials synthesis

LiV_3O_8 nanorods were synthesized by the hydrothermal reaction method, combined with a convenient solid-state reaction, as reported elsewhere [11]. In a typical experiment, the VO_2 nanorod precursor was prepared by the hydrothermal method. 0.365 g V_2O_5 powder, 10 ml 1-butanol, and 30 ml H_2O were mixed under vigorous magnetic stirring at room temperature for 4 h. The resultant mixture was then transferred into an autoclave and kept in an oven at 180 °C for 48 h. The products were washed with anhydrous ethanol and cyclohexane several times. The produced VO_2 was dried at 80 °C in a vacuum oven for 12 h. The crystalline VO_2 nanorods were obtained by annealing the dried VO_2 precursor at 250 °C for 10 h under vacuum.

The above-obtained crystalline VO_2 precursor and $LiOH \cdot H_2O$ (V/Li = 3/1.05, mol mol^{-1}) were mixed in methanol under magnetic stirring for 12 h. The mixture was heated to 50 °C to evaporate methanol. The produced powder was dried at 150 °C for 12 h in a vacuum oven, and finally annealed at 450 °C for 10 h in air. Then single-crystalline LiV_3O_8 nanorods were obtained. Polyaniline was prepared by chemical oxidation polymerization. In a typical procedure, 1.67 g aniline monomer was suspended in 50 ml distilled H_2O and stirred for 10 min to become well dispersed. Then 4.10 g ammonium persulfate in 20 ml distilled H_2O solution was slowly added to the suspension mixture. The polymerization was achieved after standing for 5 h in an iced bath, at which point the suspension becomes dark green. The products were obtained by filtering and washing the suspension with ethanol and deionized water, and then drying it under vacuum at 60 °C for 12 h.

100 mg as-prepared LiV_3O_8 nanorods were dispersed in 15 ml sodium dodecyl benzene sulfonate (SDBS) solution. Then, aniline monomer (100 mg, 200 mg, 300 mg) was added into the solution and ultrasonicated for 10 min to become well dispersed. The APS solution was then added dropwise with constant stirring to initiate the polyreaction. The reaction was carried out in an iced bath over 5 h. The final products were then filtered, washed with distilled water, and dried at 70 °C in a vacuum oven for 12 h.

2.2. Materials characterization

The PAn content in the composites was determined by thermogravimetric analysis (TGA) via a Setaram 92 instrument. Phase analysis was performed by powder X-ray diffraction (XRD) using a GBC MMA X-ray generator and diffractometer with Cu Kα radiation. PAn was confirmed by using a JOBIN YVON HR800 confocal Raman system with 632.8 nm diode laser excitation on a 300 lines mm^{-1} grating at room temperature. The morphologies of the samples were investigated by a field emission scanning electron microscope (SEM: JEOL JSM-7500FA).

2.3. Electrochemical measurements

Electrochemical measurements of the synthesized LiV_3O_8–PAn and bare LiV_3O_8 were accomplished by assembling CR2032 coin cells. The electrodes were prepared by mixing 80 wt.% active materials with 10 wt.% carbon black and 10 wt.% sodium carboxymethyl cellulose (CMC) in distilled water. The slurry was uniformly pasted on to pieces of aluminum foil with an area of 1 cm^2. Such prepared electrode sheets were dried at 90 °C in a vacuum oven for 12 h. Then, the electrodes were compressed at a rate of about 300 kPa. Coin cells were assembled in an argon filled glove box where the counter electrode was Li metal and the electrolyte was 1 M $LiPF_6$ in a mixture of ethylene carbonate (EC) and diethyl carbonate (DEC) (EC/DEC = 1:2, v/v). The cells were cycled between 1.5 and 4.0 V at a constant current density of 0.1 C (1 C = 280 mAh g^{-1}) at room temperature to measure the electrochemical response. AC-impedance measurements and cyclic voltammetry were carried out utilizing a CHI 660B electrochemical workstation. The specific capacity is based on the weight of the LiV_3O_8 or LiV_3O_8–PAn composite material.

3. Results and discussion

3.1. Structure and morphologies

The amounts of PAn in the LiV_3O_8–PAn composites were measured by thermogravimetric analysis (TGA). The samples were heated from 60 °C to 700 °C at the rate of 5 °C min^{-1}. As shown in Fig. 1, bare LiV_3O_8 maintains a constant weight as the temperature increases, while PAn begins to decompose around 300 °C and completely disintegrates at 650 °C. Therefore, for the composites, the main loss from 350 to 600 °C is assigned to the degradation of PAn, and we can calculate that the weight contents of PAn in the composites are 5 wt.%, 12 wt.% and 23 wt.%, respectively.

The X-ray diffraction (XRD) patterns of the LiV_3O_8 nanorods and the LiV_3O_8–PAn composites are shown in Fig. 2. All reflections of LiV_3O_8 nanostructured materials were in excellent accordance with the rutile structure (JCPDS No. 72-1193), which belongs to space group P21/m (11). The sharp and intense XRD peaks of the as-obtained LiV_3O_8 nanorods indicate their good degree of crystallinity. The peak at about 14° is assigned to diffraction at the (100) planes, indicating the layered structure of LiV_3O_8. These layers are composed of VO_6 octahedra and VO_5 trigonal bipyramids, which are corner sharing with the octahedral [26]. In addition, there was no notable peak shifting or intensity change after the introduction of PAn.

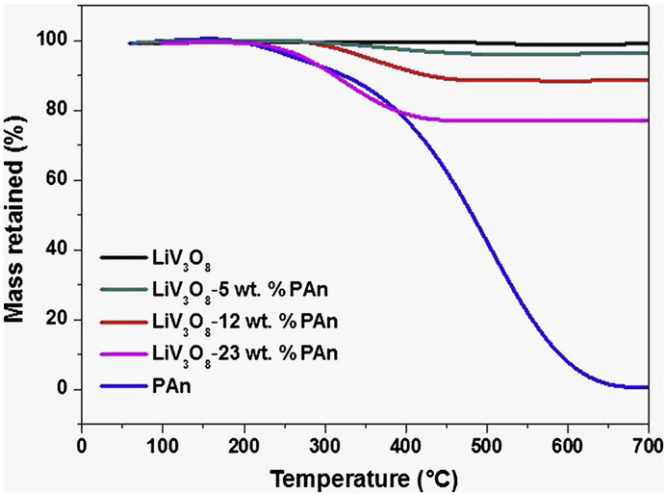

Fig. 1. TGA curves of the PAn powder, the bare LiV_3O_8 and the LiV_3O_8–PAn composites.

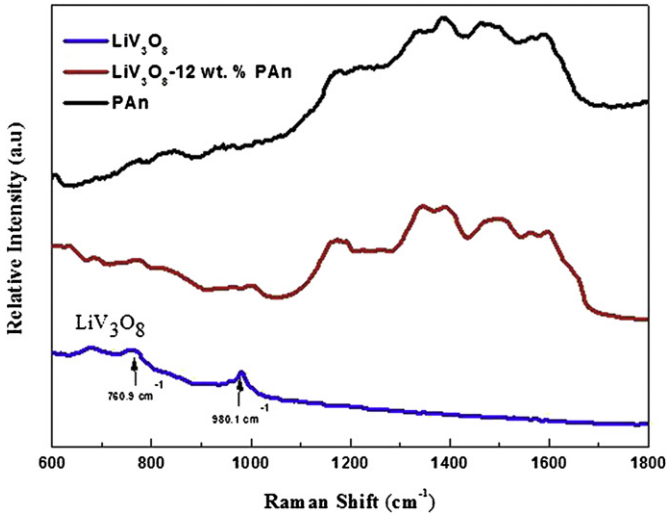

Fig. 3. Raman spectra of the PAn, LiV_3O_8 and LiV_3O_8–12 wt.% PAn composite.

Raman spectroscopy was used to confirm the presence of PAn in the composite. Fig. 3 presents Raman spectra of the composites with 632.8 nm diode laser excitation on a 300 line mm^{-1} grating at room temperature. The Raman bands of LiV_3O_8 and the composites at 980.1 cm^{-1} can be assigned to the V=O stretching vibrations of VO_5 pyramids, and the band at 760.9 cm^{-1} is likely to be related to the atomic motions of corner-sharing oxygen atoms among the VO_6, VO_5, and LiO_6 polyhedra [27]. The peaks of PAn are located between 1000 cm^{-1} and 1800 cm^{-1}, which matches up with the Raman spectrum of bare PAn [28]. This demonstrates that the LiV_3O_8 particles were combined with the PAn. No additional peaks are obvious in the Raman spectrum of LiV_3O_8–PAn, indicating that no chemical reaction between PAn and LiV_3O_8 occurred during preparation.

Typical scanning electron microscope (SEM) images of the LiV_3O_8 nanorods and the LiV_3O_8–12 wt.% PAn composite are shown in Fig. 4. The LiV_3O_8 nanorods are homogeneous with widths of 100–200 nm and lengths of 5.0–6.0 μm, and they have sharp edges. Fig. 4(b) demonstrates that the surfaces of the rods are smooth and flat, indicating complete growth of the nanorods under the experimental conditions. After the introduction of polyaniline, the LiV_3O_8–PAn composite presents a distinct contrast in the morphology. Its surface becomes rough, and the nanorod diameters increase to 200–300 nm, which confirms that the PAn is coated on the surface of the LiV_3O_8. An individual nanorod was chosen for scanning at high magnification. As seen in Fig. 4(e), the PAn layer provides good coverage of rod surfaces.

Scanning electron microscopy and energy dispersive spectroscopy (SEM/EDS) mapping of the different elements were conducted to analyze the distribution of the species within the particles (Fig. 5). The bright spots correspond to the presence of the elements N, V, and O, respectively, in which N is the element found only in PAn. Element N is distributed uniformly throughout the whole area, which indicates that the PAn has uniformly coated the surfaces of the LiV_3O_8 nanorods.

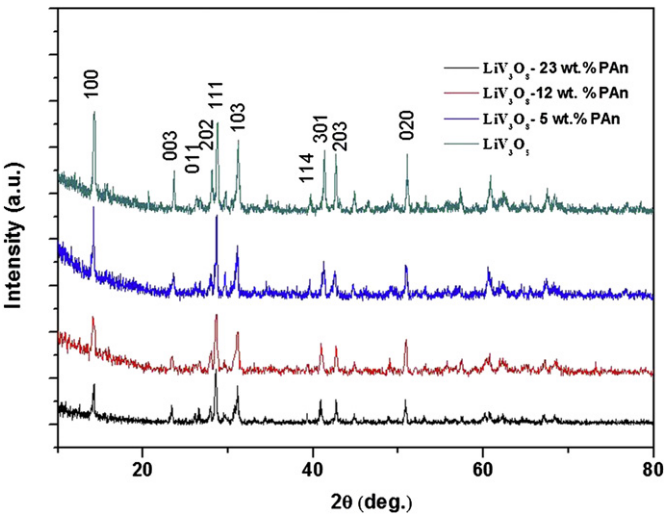

Fig. 2. X-ray diffraction patterns of the as-prepared bare LiV_3O_8 and PAn–LiV_3O_8 composites.

3.2. Electrochemical characterization

The 1st, 2nd, 5th, 50th, and 100th cycle voltage vs. specific capacity curves for the LiV_3O_8 and LiV_3O_8–12 wt.% PAn cells are presented in Fig. 6. From the charge–discharge curves of the samples, it can be seen that LiV_3O_8–PAn composite has higher capacity and superior stability in comparison with the bare LiV_3O_8 over 100 cycles. The pure LiV_3O_8 shows multistep processes in its charge and discharge curves, which are the same as those in previous reports [22,23,29]. The first specific discharge capacity of the composite is lower than in subsequent cycles, which is probably due to the activation of PAn in the charge–discharge process. This phenomenon will be discussed below.

Cyclic voltammograms of electrodes made from LiV_3O_8, composite and PAn are shown in Fig. 7. The first cycle voltammograms are rather different from the rest, indicating that some structural modifications have probably taken place during the first charge and discharge operations. There are four anodic peaks at 2.48 V, 2.79 V, 2.85 V, and 3.69 V for the bare LiV_3O_8 electrode, which is related to the deinsertion of Li^+. The main cathodic peaks of the bare LiV_3O_8 are at 1.90 V, 2.50 V, 2.74 V, 2.81 V and 3.63 V. The cathodic peak observed around 2.50 V could be attributed, based on the literature, to the two-phase transformation of $Li_3V_3O_8/Li_4V_3O_8$ [26,30,31], while the other peaks correspond to individual phase transformations [22,23]. After the introduction of PAn, the two anodic peaks at 2.81 V and 2.74 V cannot be separated anymore, the two peaks were merged into one broad peak at 2.82 V as a broad oxidation peak exists in PAn between 2.5 and 3.4 V (see Fig. 7(c)). In

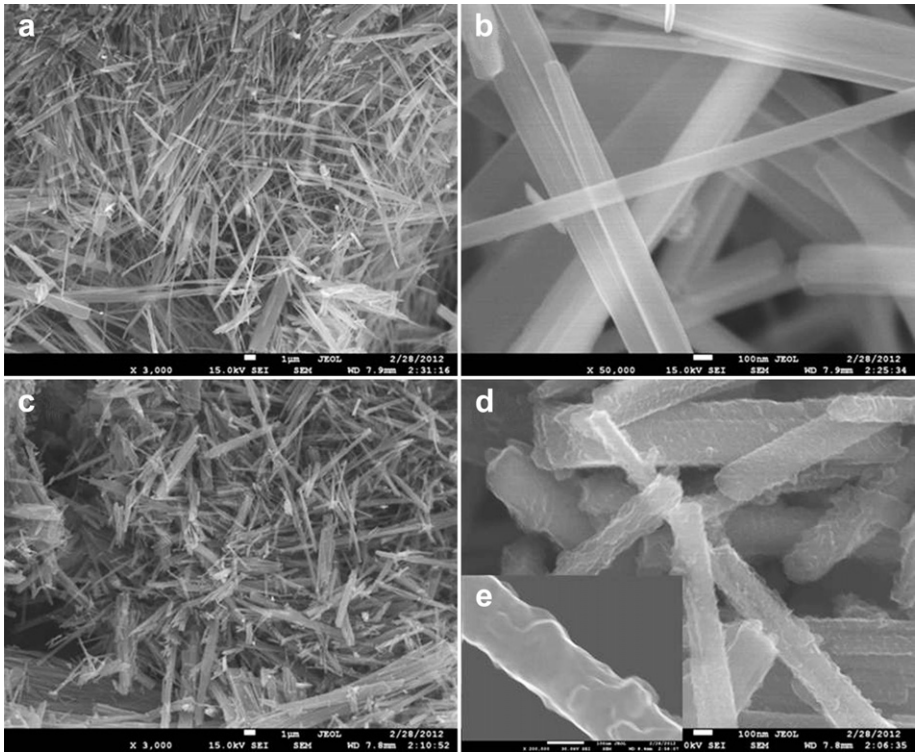

Fig. 4. SEM images of bare LiV_3O_8 (a, b), and LiV_3O_8–12 wt.% PAN composite (c, d, e).

addition, the anodic peak at 2.48 V becomes broader and appears as a shoulder in the foot of peak at 2.82 V.

Fig. 8(a) presents the specific discharge capacity of the electrodes prepared from LiV_3O_8/PAn composites, bare LiV_3O_8, and PAn, with cycling at 0.1 C. The first specific discharge capacity of PAn powder is lower than for subsequent cycles, which is probably due to its gradual activation in the first discharge process [25]. After that, the capacity of PAn becomes steady and is maintained at 62 mAh g^{-1} over 100 cycles, indicating that it is electroactive in the range of 1.5–4.0 V. The bare LiV_3O_8 electrode shows an initial

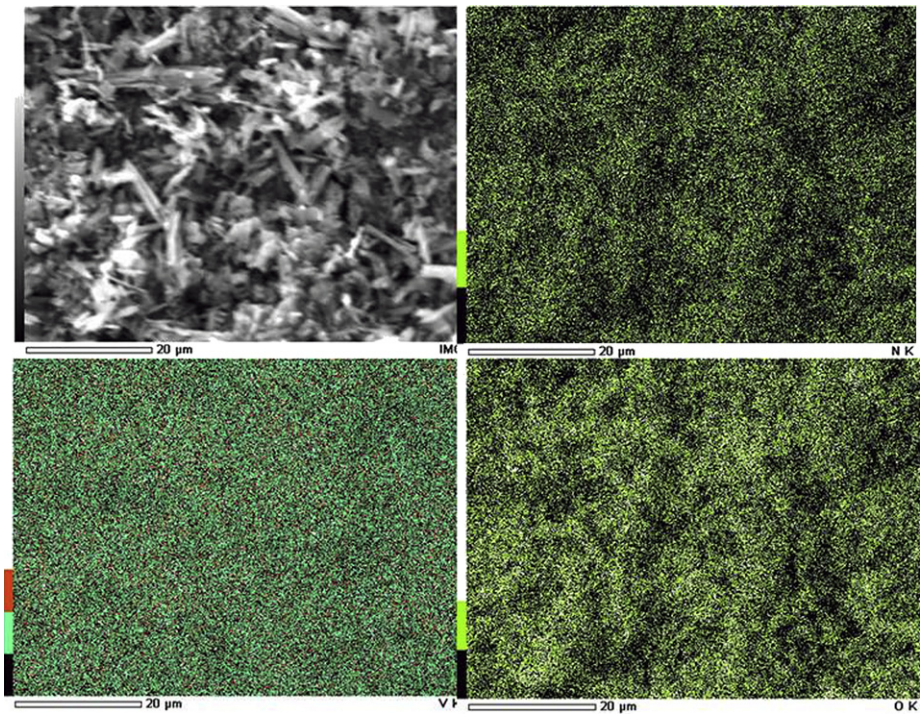

Fig. 5. SEM image (upper left) and chemical maps of N, V, and O for the 12 wt.% PAn–LiV_3O_8 composite powder.

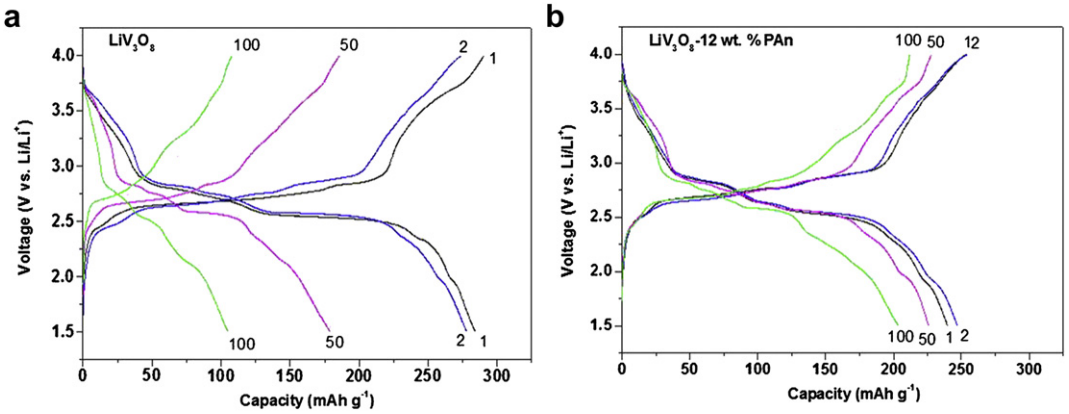

Fig. 6. Charge–discharge curves for selected cycles of LiV_3O_8 (a) and LiV_3O_8–12 wt.% PAn (b) at 0.1 C.

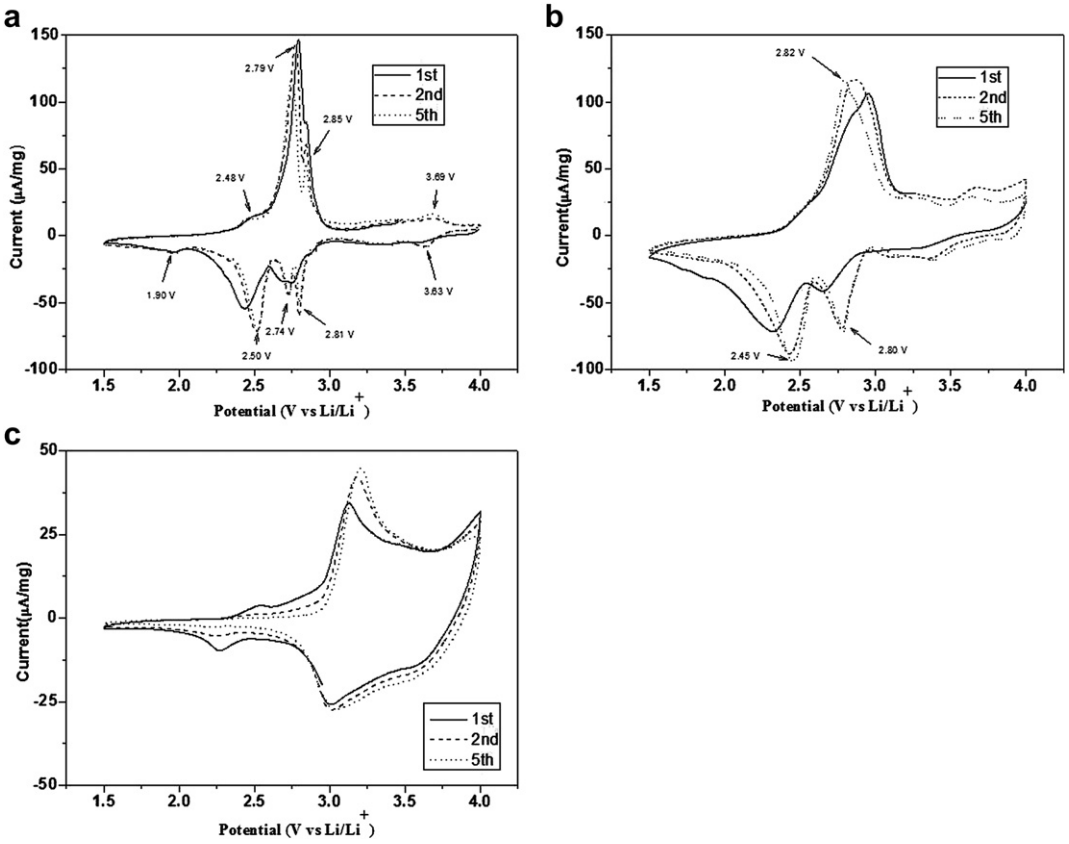

Fig. 7. Cyclic voltammograms for selected cycles of the electrodes made from: (a) bare LiV_3O_8, (b) LiV_3O_8–12 wt.% PAn, (c) bare PAn. Scanning rate: 0.1 mV s^{-1}.

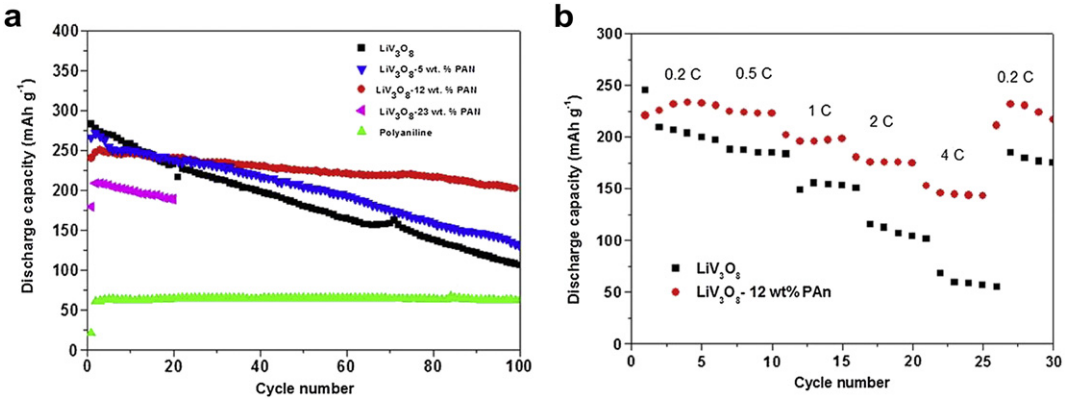

Fig. 8. (a) Cycle life of as-prepared LiV_3O_8 nanorods and LiV_3O_8–PAn composites at 0.1 C (1 C = 280 mAh g^{-1}). (b) Rate capabilities of LiV_3O_8 and LiV_3O_8–12 wt.% PAn composite with changing current densities from 0.2 C to 4 C and back to 0.2 C between 1.5 V and 4.0 V vs. Li/Li^+.

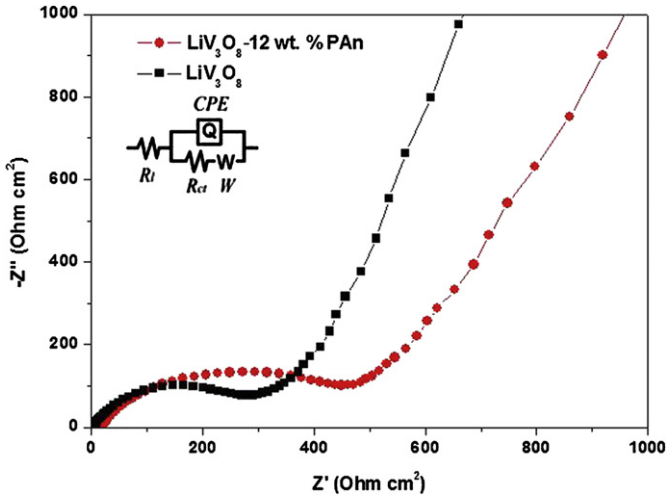

Fig. 9. Nyquist impedance plots of the bare LiV_3O_8 and the LiV_3O_8–12 wt.% PAn composite electrodes after 100 cycles. The inset shows the equivalent circuit.

capacity of 283 mAh g^{-1}. This is higher than the initial capacities of the composite electrodes, which are 186 mAh g^{-1} for LiV_3O_8–23 wt.% PAn, 243 mAh g^{-1} for LiV_3O_8–12 wt.% PAn and 260 mAh g^{-1} for LiV_3O_8–5 wt.% PAn. However, the capacity of bare LiV_3O_8 continuously decreases and declines to 108 mAh g^{-1} over 100 cycles, which is only about 38% of the initial capacity, indicating poor cycling performance. Interestingly, the discharge capacities of all the composites first increase and then reach a maximum capacity at the fifth cycle, which should be attributed to the activation of PAn. The capacity of LiV_3O_8–5 wt.% PAn reaches 130 mAh g^{-1} after 100 cycles. The composite with 12 wt.% polyaniline presents the best cycling stability, showing a specific discharge capacity of 204 mA g^{-1} after 100 cycles. This excellent electrochemical performance is comparable what was reported for LiV_3O_8/polypyrrole (183 mAh g^{-1} after 100 cycles) [22]. Further increase of PAn content in the composite would reduce the specific capacity of the composite electrode because the practical capacity of PAn is only 60 mAh g^{-1}, which is much lower than that of LiV_3O_8.

The composite with 12 wt.% PAn was chosen to test the cycling performance at different charge/discharge rates in comparison with bare LiV_3O_8. The electrode capacities were measured after 5 cycles at each rate from 0.2 C to 4 C in an ascending order, followed by a return to 0.2 C. The results are shown in Fig. 8(b). The composite presents excellent cycling stability at each rate, and the capacities are measured to be 230 mAh g^{-1} at 0.5 C, 201 mAh g^{-1} at 1C, 180 mAh g^{-1} at 2 C, and 152 mAh g^{-1} at 4 C. On returning to 0.2 C, the composite electrode delivers 250 mAh g^{-1}, which is much better than the performance of the bare LiV_3O_8 electrode (184 mAh g^{-1}). The high-rate performance is even better than that of LiV_3O_8/carbon nanosheets (110 mAh g^{-1} at 5 C and 173 mAh g^{-1} at 0.5 C) [32].

In order to explore the reasons for the good cycling performance of the composites, electrochemical impedance spectroscopy (EIS) was performed on the electrodes made from the as-obtained materials in the fully discharged state, and the results are presented in Fig. 9. The impedance curves show one compressed semicircle in the medium-frequency region, which could be assigned to charge transfer resistance (R_{ct}), and inclined line in the low-frequency range which could be considered as Warburg impedance. The values of R_{ct} for the LiV_3O_8 and the composite electrodes are 301 and 504 Ω, respectively, indicating that the PAn coating can significantly increase the electrical conductivity between LiV_3O_8 nanorods.

A morphological study of the electrodes before cycling and after 100 cycles was also conducted (Fig. 10). Fig. 10(b) is a SEM image showing the surface of the LiV_3O_8 after 100 cycles, where big cracks can be clearly observed on the surface of the electrode. For the LiV_3O_8–PAn composite electrode (Fig. 9), however, the cracks are

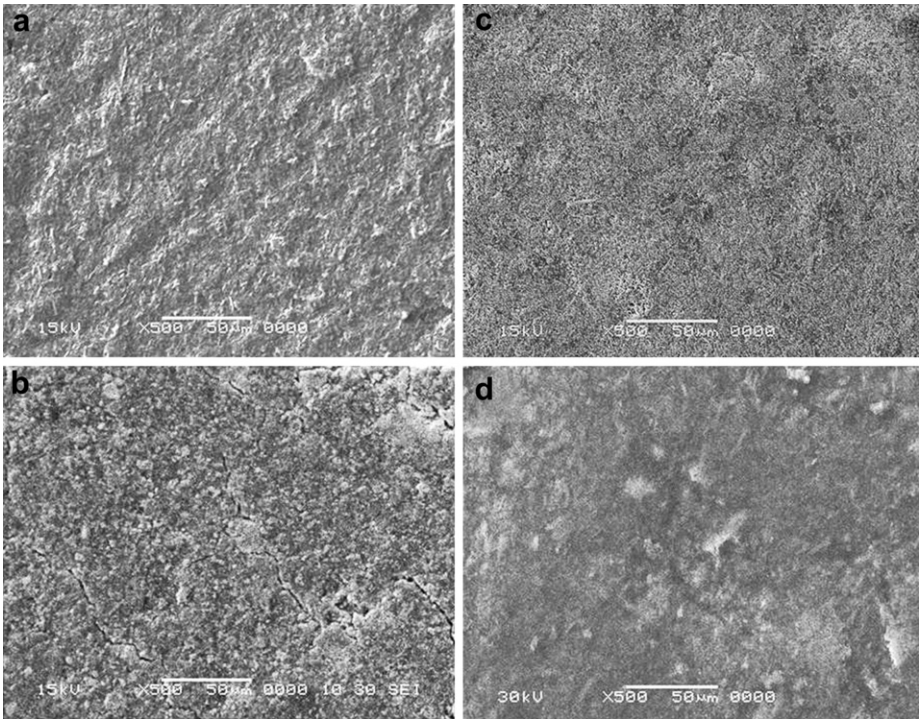

Fig. 10. SEM images of electrode surfaces of LiV_3O_8 (a, b) and LiV_3O_8–12 wt% PAn composite (c, d) before (a, c) and after (b, d) 100 cycles.

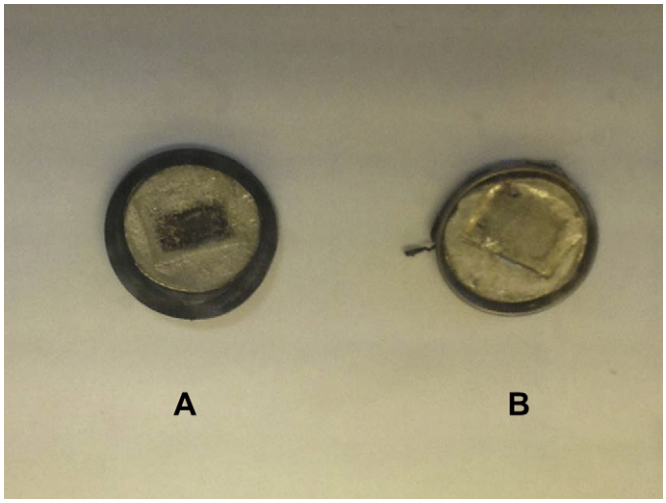

Fig. 11. The lithium anode in the cells of LiV_3O_8 (A) and LiV_3O_8–12 wt.% PAn (B) after 100 cycles.

not obvious, the integrity of the electrode is retained, and the cell just shows slight agglomeration compared to the electrode before cycling (Fig. 10(a and c)), suggesting good structural stability of the composite electrode. This excellent stability of the electrode may be attributed to the presence of the well-dispersed PAn coating on the LiV_3O_8 powders. The LiV_3O_8 structural changes during charging/discharging could be buffered by the presence of PAn. Moreover, PAn could prevent cracking and pulverization of the LiV_3O_8 electrode. At the same time, PAn can also acts as a conductive element by contributing its electroactivity, resulting in an increase in the storage capacity. Therefore, by coating with PAn, enhanced cycling stability and good high rate performance can be achieved (Fig. 11).

The cells were opened after 100 cycles to observe any differences on the lithium anode surface. Some black material was found on the surface of the lithium metal in the bare LiV_3O_8 cells. This is due to dissolution of the LiV_3O_8 particles into the electrolyte, which then migrated to the lithium anode through the separator via the electrolyte, where the reduction of vanadium ions took place. In this regard, it is expected that the dissolved vanadium complexes would be deposited on the surface of the lithium anode, which would induce a dramatic impedance rise in the cells. In contrast, the lithium foil in the composite material cell shows no such change, indicating that a uniform PAn coating on the surface of the LiV_3O_8 is an effective way to improve the cycling stability by preventing the vanadium dissolution.

4. Conclusion

LiV_3O_8 nanorods coated with conducting polyaniline are prepared by a simple chemical method. With 12 wt.% PAn coating, although a high initial discharge capacity could not be obtained, improved cycling performance and substantially improved high rate capacity have been demonstrated. This excellent electrochemical performance can be attributed to the buffering action of PAn, preventing the dissolution of active material in the electrolyte and promoting good electrical conductivity compared to bare LiV_3O_8.

References

[1] F. Bonino, S. Panero, M. Pasquali, G. Pistoia, Journal of Power Sources 56 (1995).
[2] V. Manev, A. Momchilov, A. Nassalevska, G. Pistoia, M. Pasquali, Journal of Power Sources 54 (1995) 501.
[3] S. Panero, M. Pasquali, G. Pistoia, Journal of the Electrochemical Society 130 (1983) 1225.
[4] Q. Liu, H. Liu, X. Zhou, C. Cong, K. Zhang, Solid State Ionics 176 (2005) 1549–1554.
[5] S.H. Ju, Y.C. Kang, Electrochimica Acta 55 (2010) 6088.
[6] J. Xie, J. Li, H. Zhan, Y. Zhou, Materials Letters 57 (2003) 2682.
[7] Y. Liu, X. Zhou, Y. Guo, Materials Chemistry and Physics 114 (2009) 915.
[8] M. Dubarry, J. Gaubicher, D. Guyomard, N. Dupré, C. Grey, Solid State Ionics 180 (2009) 1511.
[9] H.Y. Xu, H. Wang, Z.Q. Song, Y.W. Wang, H. Yan, M. Yoshimura, Electrochimica Acta 49 (2004) 349.
[10] G. Pistoia, M. Pasquali, G. Wang, L. Li, Journal of the Electrochemical Society 137 (1990) 2365.
[11] H. Liu, Y. Wang, K. Wang, Y. Wang, H. Zhou, Journal of Power Sources 192 (2009) 668.
[12] S. Jouanneau, A.L.G.L. Salle, A. Verbaere, D. Guyomard, Journal of the Electrochemical Society 152 (2005) 1660.
[13] Q. Gong, Y.S. He, Y. Yang, X.Z. Liao, Z.F. Ma, Journal of Solid State Electrochemistry 16 (2012) 1383.
[14] A.D. Pasquier, F. Orsini, A.S. Gozdz, J.M. Tarascon, Journal of Power Sources 81 (1999) 607.
[15] R. Vidu, P. Stroeve, Industrial & Engineering Chemistry Research 43 (2004) 3314.
[16] L. Yuan, J. Wang, S.Y. Chew, J. Chen, Z.P. Guo, L. Zhao, K. Konstantinov, H.K. Liu, Journal of Power Sources 174 (2007) 1183.
[17] J. Wang, J. Chen, K. Konstantinov, L. Zhao, S.H. Ng, G.X. Wang, Z.P. Guo, H.K. Liu, Electrochimica Acta 51 (2006) 4634.
[18] I. Boyano, J.A. Blazquez, I. de Meatza, M. Bengoechea, O. Miguel, H. Grande, Y. Huang, J.B. Goodenough, Journal of Power Sources 195 (2010) 5351.
[19] G.X. Wang, L. Yang, Y. Chen, J.Z. Wang, S. Bewlay, H.K. Liu, Electrochimica Acta 50 (2005) 4649.
[20] W.M. Chen, Y.H. Huang, L.X. Yuan, Journal of Electroanalytical Chemistry 660 (2011) 108.
[21] K. Park, H. Song, Y. Kim, Y. Kim, S. Mho, W. Cho, I.H. Yeo, Electrochimica Acta 55 (2010) 8023.
[22] S.Y. Chew, C. Feng, S.H. Ng, J. Wang, Z. Guo, H. Liu, Journal of the Electrochemical Society 154 (2007) A633.
[23] C.Q. Feng, S.Y. Chew, Z.P. Guo, J.Z. Wang, H.K. Liu, Journal of Power Sources 174 (2007) 1095.
[24] P. Novák, K. Müller, K.S.V. Santhanam, O. Haas, Chemical Reviews 97 (1997) 207.
[25] F. Cheng, W. Tang, C. Li, J. Chen, H. Liu, P. Shen, S. Dou, Chemistry – A European Journal 12 (2006) 3082.
[26] L.A. de Picciotto, K.T. Adendorff, D.C. Liles, M.M. Thackeray, Solid State Ionics 62 (1993) 297.
[27] X. Zhang, R. Frech, Electrochimica Acta 43 (1997) 861.
[28] M. Jain, S. Annapoorni, Synthetic Metals 160 (2010) 1727.
[29] L. Liu, L. Jiao, J. Sun, Y. Zhang, M. Zhao, H. Yuan, Y. Wang, Electrochimica Acta 53 (2008) 7321.
[30] J. Kawakita, Y. Katayama, T. Miura, T. Kishi, Solid State Ionics 107 (1998) 145.
[31] M. Dubarry, J. Gaubicher, D. Guyomard, N. Steunou, J. Livage, N. Dupré, C.P. Grey, Chemistry of Materials 18 (2006) 629.
[32] N.H. Idris, M.M. Rahman, J.Z. Wang, Z.X. Chen, H.-K. Liu, Composites Science and Technology 71 (2011) 343 (Artworks).